ELSEVIER

Journal of Structural Geology 30 (2008) 690–700

JOURNAL OF STRUCTURAL GEOLOGY

www.elsevier.com/locate/jsg

Evolution of a fault surface from 3D attribute analysis and displacement measurements

Tina Lohr [a,*], Charlotte M. Krawczyk [b], Onno Oncken [a], David C. Tanner [b]

[a] *GeoForschungsZentrum Potsdam Telegrafenberg, 14473 Potsdam, Germany*
[b] *Leibniz Institute for Applied Geosciences (GGA), Stilleweg 2, 30655 Hannover, Germany*

Received 5 September 2007; received in revised form 24 January 2008; accepted 7 February 2008
Available online 4 March 2008

Abstract

A large fault surface evolves by growth and coalescence of numerous segments through time, which results in strong undulations of the principal fault surface. We interpreted a strongly segmented, 13 km long fault using 3D seismic data, and studied the morphology in terms of fault linkage, using curvature, azimuth, and dip attributes. Displacement profiles of two horizons were measured to analyse the different displacement relations and to quantify their variation and dependence on fault morphology.

We identified four orders of fault segments over a scale range from a few hundred metres to several kilometres, which evolved during fault growth. The strong changes in orientation of the several segments might result in a heterogeneous small-scale fracture distribution and different fault drag geometries. Displacement measurements on the undulated fault surface indicate a strong variation between real, vertical, and horizontal displacement values. However, the commonly used throw values lead to a smoothing of the real displacement curves and to an underrepresentation of their values, and therefore cannot show a triangular shape that is typically identified from ruptures fault surfaces of earthquake processes. Therefore, for any kind of fault analysis care should be taken when using throw as approximation for the real displacement.

Keywords: Fault growth; Segmentation; Linkage; Corrugations; Seismic; Seismicity

1. Introduction

Faults grow most effectively by the coalescence of different smaller faults, whereas tip propagation is of only minor importance (e.g. Peacock and Sanderson, 1991; Willemse, 1997; Cartwright et al., 1995). Due to this coalescence of numerous segments through time, a fault's shape can strongly undulate, and the stress perturbations during fault interaction and increasing displacement result in a heterogeneous distribution of fractures at a smaller scale. Large-scale active faults are zones of potential seismicity; and together with their small-scale fracture network they can act as fluid conduits or barriers. The 3D fault shape, the linkage of a fault with other faults, and the distribution of displacement on its surface are important for defining the positions of juxtaposed beds that control, for example, sealing and permeability across faults. Consequently, for the characterisation of reservoirs, the analysis of fluid transport, the precise placement of wells, as well as for estimating the potential for earthquake generation, it is very important to have detailed information about the 3D shape of large-scale faults in the subsurface.

Undulation of a fault surface results in differences between the vertical and horizontal component of displacement, and the real displacement on the fault. Data used for investigation of fault geometry and fault statistics are often 2D (field data, remote sensing, seismic lines). Even when 3D data are available, faults are often studied in 2D only (horizon interpretation or cross-sections of 3D seismic data). However, the shape of an isolated normal fault is more complex as shown in previous

* Corresponding author. Tel./fax: +49 331 2881370.
E-mail address: lohr@gfz-potsdam.de (T. Lohr).

0191-8141/$ - see front matter © 2008 Elsevier Ltd. All rights reserved.
doi:10.1016/j.jsg.2008.02.009

papers (e.g. Walsh and Watterson, 1989; Nicol et al., 1996; Needham et al., 1996; Walsh et al., 1999).

In carrying out fault analysis, fault growth evolution is generally inferred from the geometrical characteristics of differently sized faults in the same population, rather than from kinematic analyses of individual faults. Most authors use throw as approximation for the real displacement, to analyse fault populations in terms of fault propagation through time, length vs. displacement relationship, or displacement vs. cumulative frequency (e.g. McLeod et al., 2000; Meyer et al., 2002; Walsh et al., 2002; Nicol et al., 2005). Using throw can be an approximation for displacement in case of homogeneous lithology, low fault segmentation, and smooth fault surfaces. Calculation of throw is also less time-consuming with respect to displacement, especially for investigation of large faults, or fault populations. However, as individual fault surfaces can undulate strongly, such simplified analyses might not always represent exact fault characteristics, which become more important for economic applications. The high complexity of fault growth in time and space requires a detailed analysis in 3D.

On the basis of 3D seismic data, we studied an approximately 13 km long synsedimentary fault in detail, and analysed the fault morphology and displacement distribution along the fault. We illustrate that the displacement pattern is very heterogeneous, which results in differently shaped displacement curves (triangular, half elliptical, or elliptical), depending on the displacement and its vertical and horizontal components. Additionally, the vertical and horizontal displacement, or even throw and heave values may not be representative for the real displacement along the fault because of their strong variation due to fault segmentation.

2. Database and methods

The study area is located in the NW German Basin, as part of the intracontinental Southern Permian Basin. In Central Europe, rifting and associated volcanism in the Permian occurred in a dextral transtensional stress regime (e.g. Ziegler, 1990) and produced mainly N–S striking normal faults, but also NW-trending dextral strike–slip faults (e.g. Betz et al., 1987; Ziegler, 1990; Kockel, 2002). This deformation event is well documented in our study area, expressed by grabens and halfgrabens containing Permian growth strata (Lohr et al., 2007). Sandstone, fanglomerates, and volcanic rocks have been identified by core data.

We analysed a pre-stack depth-migrated 3D reflection seismic data set, provided by RWE Dea AG, Hamburg. The line spacing of the seismic volume is 25 m, with ca. 30 m vertical resolution for the depth of the here analysed fault. We concentrated our analysis on the detailed interpretation of one synsedimentary normal fault (ca. 13 km length) and two horizons (h1 – Base Rotliegend, h2 – Top Rotliegend) (Fig. 1). The fault interpretation is based on detailed picking of every third seismic line (75 m interval) perpendicular to fault strike, numerous lines oblique to fault strike, and horizontal correlations on depth slices.

We interpreted the seismic data with the Schlumberger software GeoFrame. Triangulation of surfaces and fault attribute analyses were carried out with the software package Gocad (Gocad Consortium). The Midland Valley software 3Dmove was used for displacement measurements.

After interpretation of the seismic data in terms of horizons and faults, we created a 3D fault surface by using the Gocad triangulation method ('homogeneous triangles', Fig. 2).

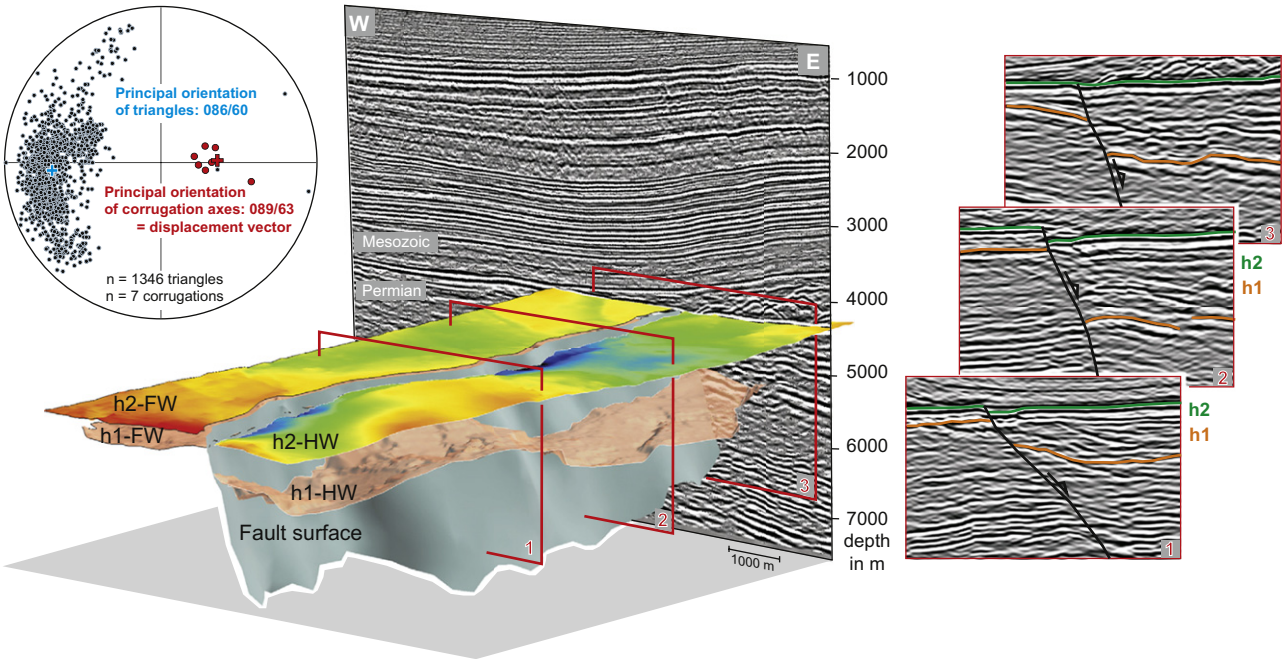

Fig. 1. 3D view showing the structural model with the analysed fault, two horizons (h1 – Base Rotliegend, h2 – Top Rotliegend), and several seismic sections. FW = footwall, HW = hanging wall. H2 horizon is colour-coded with depth from red to blue. View towards the NW. No vertical exaggeration. Left: equal-area stereonet plot of poles (lower hemisphere projection), demonstrating the variation in dip and azimuth of each fault triangle, and showing the axes of corrugations.

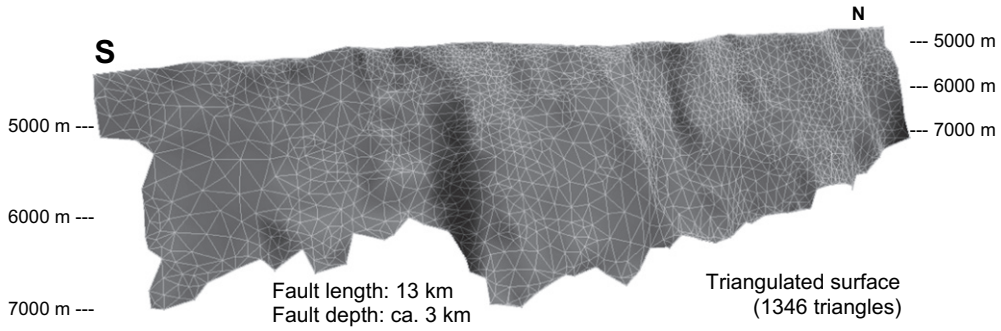

Fig. 2. 3D view of the analysed fault surface after Gocad triangulation. Surface has not been smoothed. View towards the NW. No vertical exaggeration.

Subsequently, we analysed the fault topography by using the attributes dip, azimuth, and curvature. The dip and azimuth are calculated from each triangle of the fault surface. The Gaussian curvature at a given point is the product of the two principal maximum and minimum curvatures. By flattening the 3D triangular grid, positive curvature is defined by a gap forming between flattened triangles of a dome, whereas negative curvature is defined by an overlap forming between flattened triangles of a saddle or basin. Surfaces with a high Gaussian curvature like domes or saddles are non-cylindrical, whereas cylindrical surfaces like elongated folds have a Gaussian curvature of zero (Lisle, 1994).

The attributes dip, azimuth, and curvature can highlight corrugations on the fault surface. These attributes vary independently from the sections on which the fault has been interpreted, and are therefore a real feature rather than an artefact of the interpretation. Such fault corrugations are assumed to result from segment linkage (e.g. Walsh et al., 1999; McLeod et al., 2000; Mansfield and Cartwright, 2001; Marchal et al., 2003). Other explanations to what else these corrugations might be related to could be: compression parallel to fault strike and subsequent folding of the fault surface, but also pre-existing fracture sets or sedimentary features. These possibilities can be excluded here because in the studied example there is no evidence for a later folding or for any pre-existing fabric because the fault grew synsedimentarily.

It is also generally assumed that corrugations indicate the movement direction as parallel to their axes because this movement direction will require least energy and therefore smallest strain (Needham et al., 1996). Such corrugations have been observed also in the field (e.g. Wright and Turner, 2006; Sagy et al., 2007), and can be interpreted as fault segments and fault segment linkage zones. Striation measurements on these corrugations evidenced that corrugations are parallel to fault slip (Hancock and Barka, 1987). These corrugations observed in the field might be comparable to those observed in seismic data.

Thus, we used the here observed corrugations to define the displacement vector on the fault. For the subsequent displacement measurements we calculated the magnitude of horizontal, vertical, and real displacement between the two Permian horizons: we mapped in detail the positions of the hanging wall and footwall cut-offs on the fault surface (by directly ''snapping'' in the seismic interpretation software), defined the movement direction on the fault from the fault corrugations (average movement direction is 089°, see stereonet plot in Fig. 1), and subsequently measured the displacement and its horizontal and vertical components using the 3Dmove module ''Allen Mapper''. For this purpose, a vertical plane trending parallel to the movement direction was shifted step by step along the fault, rasterising the fault in numerous cross-sections (180 cross-sections at h1, and 250 cross-sections at h2) and measuring the displacement magnitudes.

After Peacock et al. (2000, and references therein) a simplified measure for horizon separation, obtained in a plane parallel to fault dip, is *dip separation* (Fig. 3), in which slip represents the horizon separation in a straight line on a fault surface, and throw and heave are its vertical and horizontal components. For our analyses we use the term *real displacement* for the relative movement between two originally adjacent points on the fault surface following its undulations (Fig. 3), according partly to the terminology of Peacock et al. (2000, and references therein). Consequently, we determined the displacement vector by (1) using the orientation of corrugation axes as movement direction, and (2) taking the amount of horizon separation parallel to movement direction as a curved line following fault surface undulations. In our 3D analysis the displacement vector indicates that the here analysed fault is a dip-slip normal fault, because corrugation axes are nearly parallel to fault dip (stereonet plot in Fig. 1). Therefore, the dip separation components throw and heave are similar to the vertical and horizontal displacement components.

3. Fault analysis

The studied fault strikes N–S and dips toward the east (Fig. 1). The fault is accessible almost in its complete extent in the seismic data set. The northern bound is limited by the margins of the seismic volume, whereas the southern bound is limited in interpretation by an overlying Zechstein salt diapir. The fault is picked in a depth from 4200 m down to 7500 m (Fig. 2); the minimum value is defined by the blind upper fault tip because of the end of deformation, and the maximum value is given by the depth limit of the seismic volume (Fig. 1). The southernmost part of the investigated fault

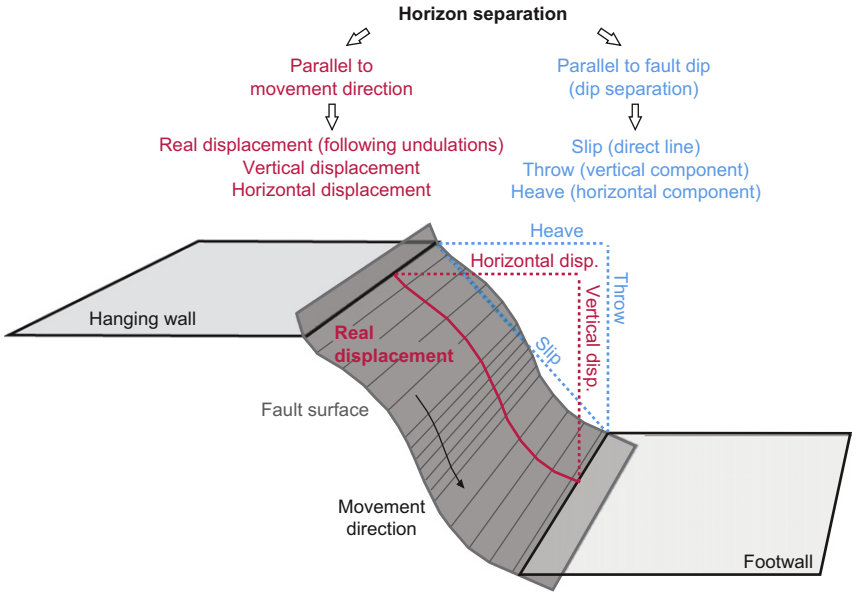

Fig. 3. Sketch with horizon hanging wall and footwall, and fault surface, illustrating the relation between the different possibilities of horizon separation: parallel to fault dip and parallel to movement direction. Terminology after Peacock et al. (2000, and references therein). In our analyses we measured real displacement, vertical displacement, and horizontal displacement.

has been affected by later faulting. These areas were not involved in our analysis.

We studied the fault morphology (Fig. 2) in two different ways: fault attribute analysis (dip, azimuth, curvature) highlights fault corrugations in 3D at a larger scale of several kilometres. In contrast, displacement measurements can emphasise fault corrugations only in 2D, but on a smaller scale of a few hundred metres to several kilometres. The results of both methods are appropriate to analyse the fault morphology over a larger scale spectrum.

3.1. Large-scale fault analysis

Analysing the fault morphology in 3D, we observed an undulation of the whole fault (Figs. 1 and 2), expressed already by differences in orientation of the numerous fault surface triangles.

The *dip* and *azimuth* maps and their histograms illustrate these differences (Fig. 4). The fault dip varies between 35° and 80°. The average dip is 60°, but there are two main clusters with an average dip of 42° and 65°, respectively. The average azimuth is 086°, but it varies between 040° and 165°. Comparing the dip and azimuth histograms (Fig. 4) with the dip–azimuth pole plot (Fig. 5) it is possible to assign fault regions to clusters of the pole plot. Density contour lines highlight several clusters (1–4), which correspond to several dip or azimuth clusters in the histogram, and to several regions in the fault attribute maps: cluster 1 corresponds to the majority of high-dip areas in the north and the south, cluster 2 is the low-dip area in the middle of the fault (overlap zone), cluster 3 represents the southernmost parts of both second-order faults (explained in Section 3.2 '*Small-scale fault analysis*'), and cluster 4 is related to a possible transfer zone (explained in Section 4.1 '*Fault corrugations and displacement calculations*').

The Gaussian *curvature* was calculated for the whole fault surface. The undulation of the fault surface is not homogeneous in both directions, but it is elongated sub-parallel to fault dip, and the fault can therefore be described as a cylindrical surface. For that reason we used the minimum Gaussian curvature since it highlights well the corrugations on this surface (Fig. 4). Areas of positive curvature are convex to the hanging wall, and represent areas where fault linkage occurred. Areas of negative curvature are concave to the hanging wall, and represent the fault segments itself (Fig. 4). In the histogram the average minimum local curvature is shifted to more negative values, which means that concave areas, and thus fault segments, are overrepresented with respect to the convex ones (fault linkage areas). That is reasonable as fault segments are usually larger than zones of fault linkage. The high curvature areas are not continuously visible along fault depth. Comparing both, dip and curvature map, indicates that areas of high negative curvature are represented by higher dip, with respect to their surroundings, and that corrugations become narrower or die out towards the depth; some of them even at the same depth level of about 6000 m (Fig. 4).

Subordinate to these vertical corrugations we also note horizontal corrugations (Fig. 4, e.g. at ca. 5000 m depth level between 7000 and 10,000 m distance along the fault). The hanging wall and footwall cut-off lines often match with areas of strong changes in dip or curvature, e.g.: the large horizontal corrugation visible as a low-dip area within the northern part of the fault is located between the hanging wall and footwall cut-offs of horizon h1; the hanging wall cut-off of this horizon often limits areas of high negative curvature at depth (Fig. 4, e.g. at 3600, 7400, 8900 m distance along the fault). The

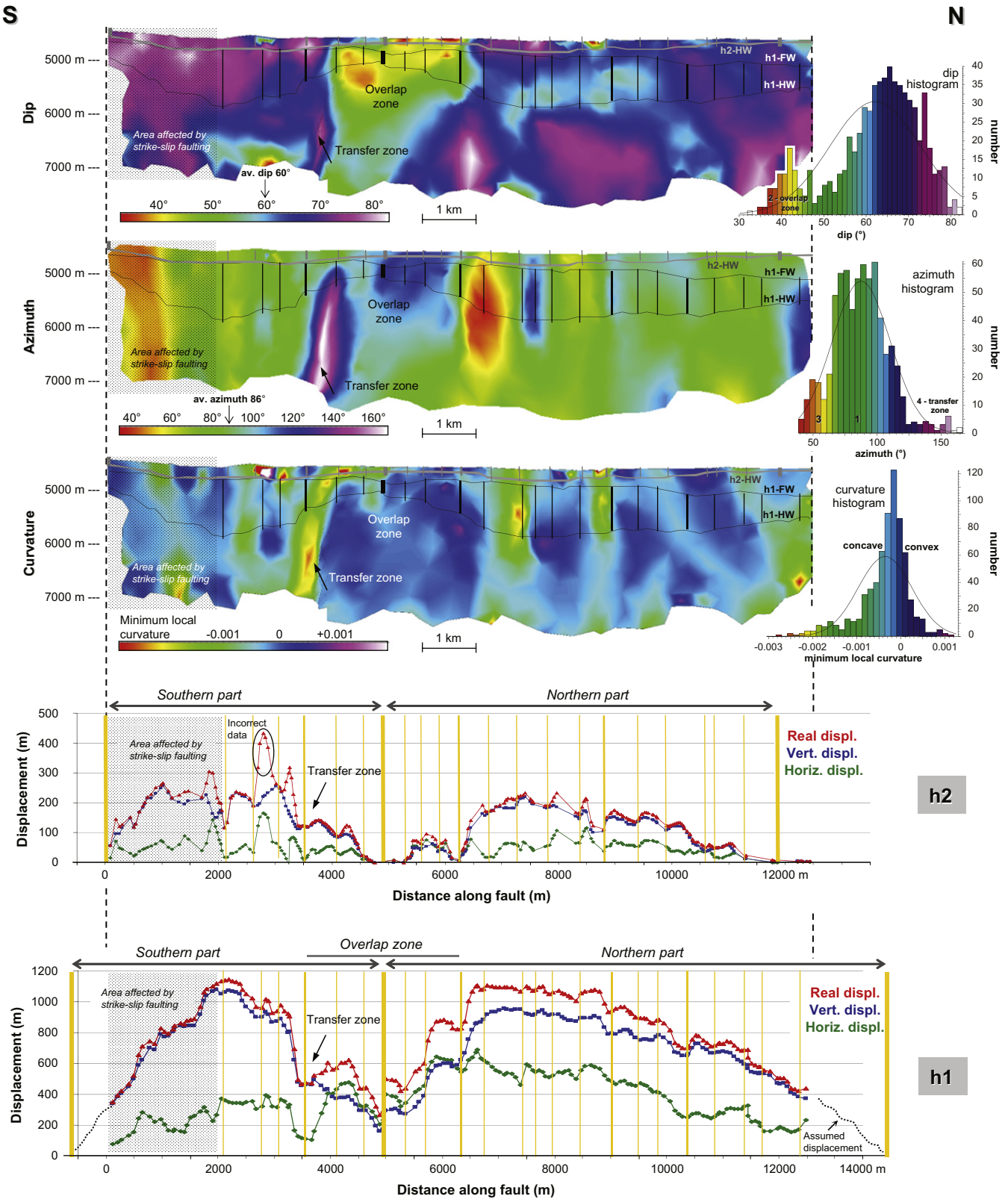

Fig. 4. Top: fault surface as colour-coded attribute maps showing dip, azimuth, and curvature, with corresponding histograms. View towards the fault surface. Horizontal undulated lines are hanging wall and footwall cut-off of h1 (black lines, h1-HW and h1-FW), and hanging wall cut-off of h2 (grey line, h2-HW). Straight vertical lines between the cut-offs represent segment boundaries interpreted from the diagrams below. Numbers in histograms are related to the clusters in Fig. 5. Below: displacement–distance diagrams of the two Permian horizons (h1 – Base Rotliegend, h2 – Top Rotliegend) showing their separation along fault. Coloured lines indicate real displacement (red), vertical displacement (blue), and horizontal displacement (green). Variations of these lines reflect different fault segments, which have been linked during fault propagation and finally produced one large fault surface. Vertical yellow lines in the diagrams are fault segment boundaries. Segments between thinner lines are smaller and older, whereas segments between thicker lines are larger and younger segments, which developed from linkage of the smaller ones. According to this subdivision four generations of fault growth are identified.

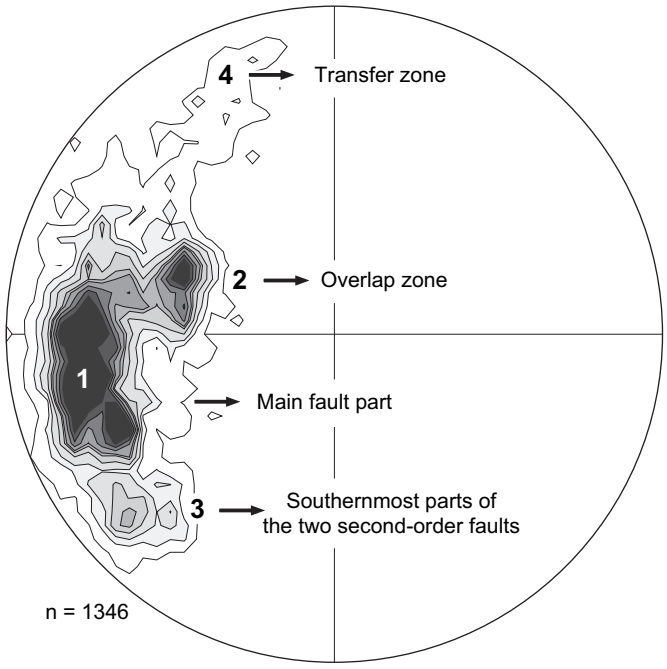

Fig. 5. Equal-area stereonet plot with contour lines shows the distribution in orientation of fault surface triangles derived from pole point plot in Fig. 1. The four identified clusters have been correlated with areas on the fault surface (compare with Fig. 4).

uppermost part of the fault surface (the area between hanging wall and footwall of horizon h2) is characterised by several small areas of changes in dip and curvature. This implies higher fault roughness in this upper part compared to deeper areas.

3.2. Small-scale fault analysis

For a more detailed investigation of fault corrugations, we measured the displacement of two horizons (h1 – Base Rotliegend, h2 – Top Rotliegend) along the fault. We analysed the amount of the real displacement, and its vertical and horizontal components. The results are shown in the displacement–distance diagrams (Fig. 4) that illustrate the displacement variation parallel to fault strike. Profiles of both horizons are asymmetric, triangular to elliptical, convex shaped curves. The displacement varies between 0 and 1200 m in h1, and between 0 and 300 m in h2. The curves show several sub-units with local minima and maxima, which point to different segments, that merged during fault growth. Maxima represent the core of the fault segments because maximum displacement occurred close to the centre of the segments, whereas minima represent areas where fault segments are linked because displacement is tapering off at the edges. Minima are also characterised by abrupt changes in displacement. Their positions are similar in all three curves, but the amounts are different between these curves, which results in a different relationship between real, vertical, and horizontal displacement of each segment. Based on the distribution of minima and maxima, we identified four generations or orders of segments on both horizons (Fig. 4). These are younger with increasing fault length, because of progressive fault growth by segment linkage.

Fourth-order: more than 23 small-scale segments (200–700 m length).
Third-order: at least six medium-scale segments (1.5–3 km length).
Second-order: two large-scale segments (5–9 km length).
First-order: one large-scale final fault (ca. 13 km length).

Vertical yellow lines in the diagrams separate these segments. Segments between thinner lines are smaller and older, whereas segments between thicker lines are larger and younger segments. The first-order fault has a length of approximately 15 km at horizon h1, and 12 km at horizon h2. The two second-order faults are well visible on the present-day morphology of the h2 hanging wall (Fig. 1). Here, the depth map shows two areas of increased depths (blue coloured), which indicate maximum subsidence and displacement along horizon h2 (fault controlled depocentres). The area between both second-order faults appears as overlap zone, bounded by a transfer zone to the south (Fig. 4). Third-order faults are in the scale of a few kilometres, and the numerous fourth-order faults with several hundred metres length are the smallest segments that could be identified by this method.

Areas of segment linkage identified from the displacement–distance diagrams match with areas of strong differences in dip, azimuth, or curvature, identified from fault morphology analysis (Fig. 4). In the dip map the vertical lines often separate neighbours of varying dip. The colour bar of the azimuth map highlights especially areas which strike oblique to the major fault, so that green coloured areas represent mainly fault segments. In the curvature map, most of the fault segments are directly visually enhanced by the negative curvature values presented in red, yellow and green colours. Nearly all segment boundaries from the diagrams have been identified also on one or more fault attribute maps. However, a few fourth-order segments could not be correlated with fault attribute maps. This might be because the displacement–distance diagrams can identify fault segments on a much smaller scale. In general, the fault surface roughness seems to change with depth. The upper part of the fault surface between the hanging wall and footwall of h2 is characterised by a higher amount of small fault segments with respect to the area of h1. In h1 small segments can only be identified in the displacement–distance diagram in such detail, but rarely on the attribute maps.

The fault morphology, especially the changes in dip, controls the real displacement-to-vertical displacement ratio. We calculated this ratio for the oldest horizon h1 (Fig. 6). Here, the ratio varies along fault strike between 1 and 1.8. The curve is strongly undulated and describes mainly concave shapes, which are separated by local maxima. These local maxima can be correlated in most cases with zones of segment linkage derived from the displacement–distance diagram (Fig. 4). The highest real displacement-to-vertical displacement ratio occurs within the large overlap zone, in which the second-order fault

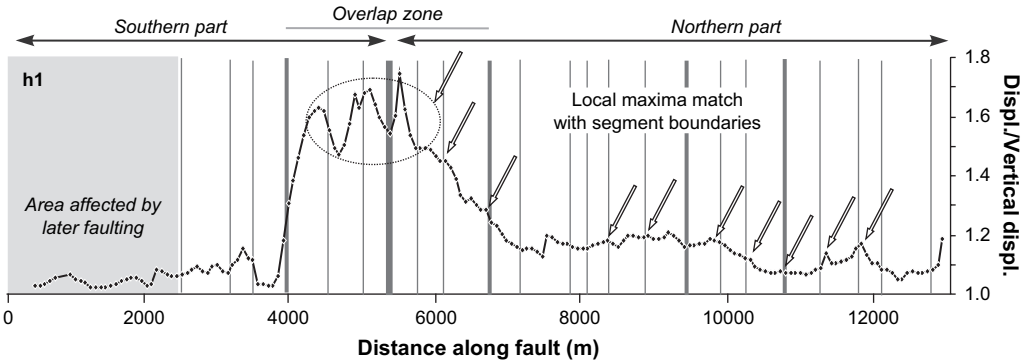

Fig. 6. Real displacement-to-vertical displacement ratio of horizon h1. Vertical lines are segment boundaries derived from the displacement–distance diagram in Fig. 4. In general, high ratios point to segment boundaries, whereas low ratios indicate fault segments. Here, arrows mark such maxima that correlate with segment boundaries.

segments are linked. The reason for this correlation is that fault segment boundaries have typically lower fault dip and smaller displacement with respect to the segment centre, which results in a higher real displacement-to-vertical displacement ratio.

Fig. 7 shows the amount of vertical and horizontal displacement with respect to the real displacement of all data pairs from the sections along both horizons. Comparing the three curves indicates that they are not sub-parallel as it would be the case on a planar fault surface. Instead, the vertical and horizontal displacements strongly undulate in comparison to the real displacement. In some cases, the horizontal displacement is even higher than the vertical one. This occurs when the fault dip is locally below 45°, as it is the case in the area of the overlap zone (see dip map in Fig. 4). The higher the differences between vertical and horizontal displacement, the steeper the fault is. The heterogeneity in the curves is mainly caused by fault segmentation and the related undulation of the fault surface. Additionally, the real displacement curve in this diagram (Fig. 7) is not a continuous line, but it is marked by steps of some tens of metres. These steps divide the curve into groups of similar real displacement, but the

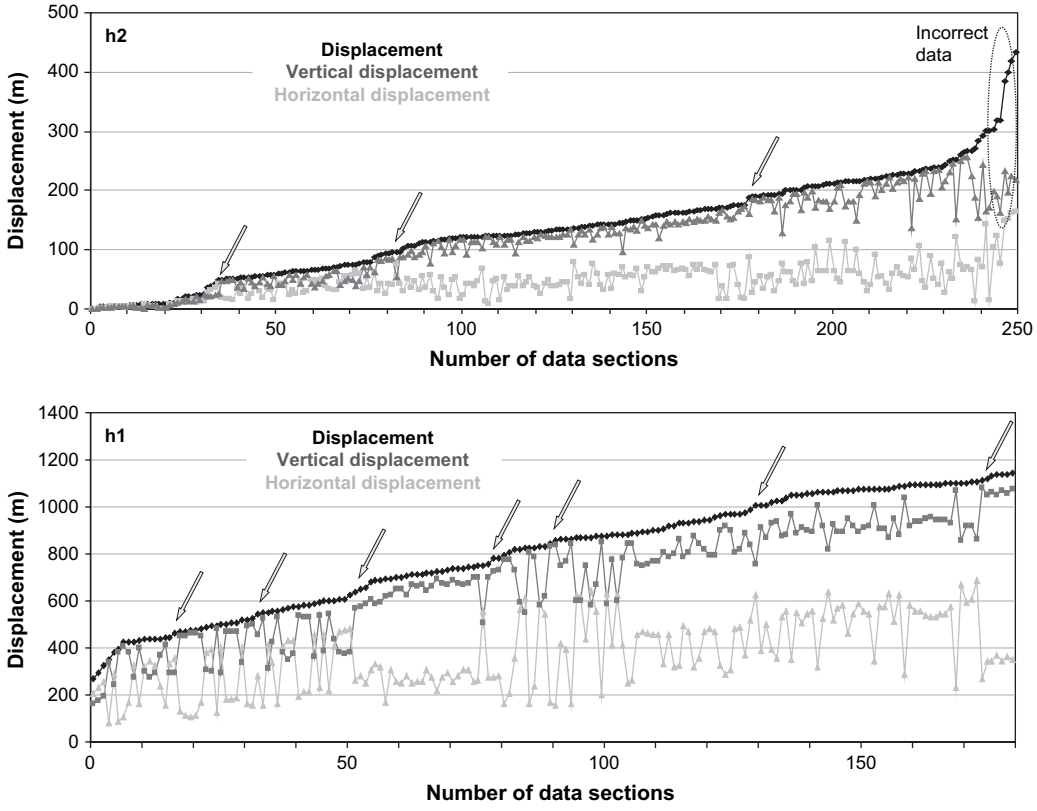

Fig. 7. Variation of vertical and horizontal displacements with respect to real displacement. Data pairs from the sections of both horizons are ordered by real displacement. Steps in curve represent groups of segments with similar real displacement pattern.

relation between the vertical and horizontal displacement often varies.

4. Discussion

4.1. Fault corrugations and displacement calculations

With the here used methods of 3D fault interpretation and subsequent attribute analysis and displacement measurements, we identified corrugations as former segments on a present-day large fault surface, over a scale range from a few hundred metres to several kilometres. The results can be correlated over that range of scales and demonstrate the validity of the two methods. We assume that the here analysed fault formed from smaller faults, which coalesced during fault propagation in the Permian.

On a km-scale attribute analysis of the fault surface highlights undulations, especially corrugations, which we interpret to represent former fault segments and fault linkage areas. Areas of negative curvature, which are concave to the hanging wall, are interpreted as fault segments. Areas of positive curvature, which are convex to the hanging wall, are interpreted as breached relay zones where fault linkage occurred. One example of negative curvature even highlights a possible transfer zone, which might indicate a breached relay ramp (Fig. 4). The fault corrugations identified by attribute analyses are sub-parallel to fault dip, and are assumed to be aligned parallel to movement direction (also Needham et al., 1996).

By displacement analysis on a scale of a few hundred metres to several kilometres we identified four orders of segments illustrating different fault generations, getting younger with increasing fault length. Each segment has its own real displacement–vertical displacement–horizontal displacement relationship, which is mainly caused by differences in fault strike and dip along both fault strike and fault depth (compare displacement–distance diagrams with fault attribute maps in Fig. 4). Differences along strike are caused by lateral coalescence of several segments (see also Needham et al., 1996; Marchal et al., 2003), whereas differences towards depth might be caused by vertical coalescence of several segments (Mansfield and Cartwright, 2001; Marchal et al., 2003), or by lithological inhomogeneities (Crider and Peacock, 2004), or a combination of both.

Our analyses show that the fault surface topography evolves with increasing displacement. Since we observed a variable fault roughness associated with the horizon cut-offs rather than with depth, we assume that this roughness is related to displacement, rather than lithological inhomogeneities, or even interpretation uncertainties due to lower resolution at depth. In the here analysed scale the fault smoothes with increasing displacement. Therefore, we assume that coalescence of several segments leads first to an increase in fault roughness, whereas during maturation the fault surface becomes smoother. From outcropping fault surfaces analysed by laser scanning Sagy et al. (2007) also implied that mature fault surfaces are smoother, and that displacement correlates with fault roughness.

The displacement curves of the second-order, and partly the third-order segments are characterised by an asymmetric shape. The overlapping fault tips have steeper displacement gradients than the corresponding distal tips (Fig. 4). This asymmetric fault growth is caused by different fault length propagation at both sides of the fault. During length propagation, the overlapping tips are hampered, but the free ends of the faults do propagate normally, as well as the growth in displacement is the same. This distortion of the displacement profile is typically observed in fault interactions (e.g. Peacock and Sanderson, 1991; Scholz, 2002).

The asymmetry in displacement distribution of the smaller segments is caused by a higher displacement in the centre of the superimposed fault. The positions of displacement maxima are similar in both horizons, and the positions of third- and fourth-order segment boundaries are mainly coincident. However, the first-order fault boundaries do not match, because the fault length is smaller at the younger horizon h2 (12 km), than at the older horizon h1 (15 km) (Fig. 4). That indicates that in this observable deformation stage, the fault propagated only in displacement, but no tip propagation at the free ends of the fault has occurred.

4.2. Implications for fault drag, scaling, fracture prediction, and seismic hazard assessment

The variable displacement along fault strike caused by segment linkage, and the variable displacement relations caused by differences in segment orientation, can result in heterogeneous deflections of horizons close to the fault, and should therefore have an influence on different fault drag geometries along the fault (reverse or normal drag).

Fault drag geometries and flanking structures have been described and analysed by, e.g., Barnett et al. (1987), Passchier (2001), Exner et al. (2004), Coelho et al. (2005), Grasemann et al. (2005) and Wiesmayr and Grasemann (2005) on field outcrop scale or analogue and numerical modelling. These authors suggested that different drags result from a local decrease or increase in displacement, and that the sense of fault drag (reverse or normal) is mainly a function of the angle between the horizon and the fault plane, and therefore of the variation in fault dip. That means that areas of lower displacement and lower fault dip like linkage areas should show normal drag, whereas areas of higher displacement and higher fault dip like segment centres are characterised by reverse drag. Such a variation of different fault drags has been partly observed along the here investigated fault. However, for a systematic identification of areas of reverse and normal drag it would be necessary to map the fault–horizon geometry in detail, to analyse the angle between fault and horizon, and to measure the curvature of footwall and hanging wall close to the fault for identifying changes in their concave and convex shapes.

Grasemann et al. (2005) stated the scale independence of reverse drag and rollover-like geometries, and argued for the reverse drag model as alternative to the concept of rollover anticlines which generally form above listric extensional faults.

Because reverse drag develops as a result of heterogeneous displacement, a rollover-like geometry in the hanging wall does not necessarily imply a listric fault in depth (Grasemann et al., 2005). Possible fault drag structures of the here analysed fault are on a scale of several tens to a hundred of metres. A detailed study of such a large-scale seismic fault surface focusing on fault drag geometries could further verify the alternative reverse drag model by Grasemann et al. (2005) even on a large-scale, and would underscore the importance for quantifying regional extension.

Care should be taken when calculating the length vs. throw or heave relationships, throw or heave vs. cumulative frequency relationships, and throw or heave through time, especially for a predictive purpose. An ideal self-similar growth is rarely observed; in general, there is a lot of scatter in throw or heave vs. length correlation plots, which is caused by the process of segment linkage (Cartwright et al., 1996; Mansfield and Cartwright, 2001), and partly also due to the use of throw and heave values rather than the real displacement. Because of strong differences in real displacement, vertical and horizontal displacements, and even throw and heave of mature, high undulated faults, it is necessary to use real displacement values as they represent the true movement along the fault. Otherwise, the use of vertical and horizontal displacement or even heave and throw values leads to underestimation of the fault's displacement. To work out the precise effects, it would be necessary to calculate the length vs. real displacement relationship over time for all segments of one fault. However, in a segmented fault, the original lengths and displacements of the several segments are difficult to reconstruct, because they are underrepresented due to linkage. The present-day observable fault lengths and fault displacements in the displacement–distance diagram are slightly smaller than in reality, because they are related to a certain horizon that may not indicate the beginning of deformation. The solution would be to interpret for each segment that horizon which documents the beginning of faulting. However, in our example there is a lack of continuous and datable horizons for doing such detailed interpretations. Furthermore, the here analysed fault is not large enough for documenting a statistically relevant number of fault segments. For these reasons, it was not possible to demonstrate specific implications on the scaling law between e.g. length vs. real, vertical and horizontal displacements, slip, throw, and heave in the here introduced example.

According to the inhomogeneous fault roughness, the rocks around the fault should show an inhomogeneous strain field with high fracture concentration in areas of strong fault undulations (high curvature) (Lisle, 1994). Fault zones of high curvature are affected by higher deformation, and are therefore characterised by a higher fracture density. Hence, a large segmented fault shows a variable fracture density along both fault strike and fault depth. From fault analysis on the here studied scale, it might be possible to make qualitative predictions about fracture density around the major fault also on a much smaller scale, e.g. below the seismic resolution down to a few metres or even well data scale. This finally helps to localise strongly fractured zones, which is important for analyses of fluid migration and for reservoir characterisation.

Our analyses show triangular to half elliptical shaped displacement profiles, clearly visible in real displacement, but rather unclear in vertical and horizontal displacement. A triangular shape of displacement profiles is considered typical for long-term slip profiles derived from multiple rupture surfaces from earthquake processes (e.g. Nicol et al., 1996; Manighetti et al., 2001; Manzocchi et al., 2006). However, this triangular shape from seismological analyses has not been shown by analyses from seismic data; instead, in these studies fault growth is typically characterised by an elliptical to half elliptical throw curve (e.g. Meyer et al., 2002; Nicol et al., 2005; Bull et al., 2006). A reason for this discrepancy could be that fault growth evolution has generally been inferred from the geometrical characteristics of faults of different size in the same population, rather than from kinematic analysis of an individual fault. Displacement profiles of one single mature fault change continuously through time due to segment linkage. Neighbouring faults act as barriers and hamper tip propagation, which results in a higher displacement gradient and necessarily in a more triangular curve. However, the often used throw values generate only an elliptical to half elliptical shape due to underrepresentation of real displacement despite constant fault length, as it is illustrated in our displacement profiles (Fig. 4). Additionally, the use of 2D seismic profiles, instead of a complete 3D interpretation, lowers the sampling rate significantly, which results in (1) a smoothing of the real displacement curve, (2) an incomplete identification of fault segments, and (3) a nearly impossible recognition of a potential triangular shaped curve. In the latter case, a triangular curve can only be identified in 2D profiles by choosing the exact position of maximum displacement, and in addition numerous profiles around to prove the displacement gradient towards the fault tip. With this method, a triangular curve can only be identified by chance.

Analyses of the morphology of large faults are important for the improvement of seismic hazard assessment. From seismological data, inhomogeneities on large-scale fault surfaces are known as asperities. These asperities are described as areas of higher resistance against the general motion, caused by structural heterogeneities or varying material properties (Sobiesiak et al., 2007). During rupturing of asperities, these areas are characterised by an increased seismicity and higher slip values. Fault morphology analyses could help to identify areas with high earthquake potential of seismic active faults, and to elucidate better the rupture process along the surface. However, for testing the comparability of the fault surface roughness with the seismological potential, it is necessary to apply both analyses, 3D seismic and seismological data, on a single large-scale fault in very detail. If areas of increased displacement correlate in both methods, and areas of segment linkage correlate with asperities, then the here presented morphology and displacement analysis is an important contribution for the improvement of seismic hazard assessment.

5. Conclusions

In this paper we demonstrate fault analysis of a ca. 13 km long segmented fault, derived from detailed interpretation of a high-resolution 3D seismic data set. Here, we present for the first time the evolution of fault segmentation on a single normal fault, with the combined methods of morphology analysis and displacement measurements. We identified four orders of segments on two horizons getting younger with increasing fault length, over several scales from 200 to 15,000 m fault length. Fault attribute maps (dip, azimuth, curvature) and displacement diagrams emphasise changes in fault strike and fault dip of the fault surface. Our analysis shows a strong variation in real, vertical, and horizontal displacements, especially in areas where fault segments are linked. The difference in the amount of displacement increases with undulation along fault strike and fault dip. Consequently, the vertical and horizontal displacement, or even throw and heave values should not regularly be used as approximation for the real displacement, as they are not always representative for fault analysis of large segmented faults (e.g. fault propagation through time, throw and heave vs. length or cumulative frequency). Otherwise, high amounts of real displacement will be underrepresented.

Fault morphology analyses of large-scale faults can be important for improvement of seismic hazard assessment, as the fault roughness is possibly associated with the heterogeneous distribution of earthquake data. The here presented real displacement curves are characterised by a triangular to half elliptical shape, rather than being elliptical. We assume that the use of 2D profiles instead of 3D data, and the use of throw and heave instead of real displacement, leads to an incomplete identification of fault segments, and therefore results not only in a smoothing of the curves, but also in a change from triangular to (half-) elliptical curves. Hence, the high complexity of fault growth in time and space requires a detailed analysis in 3D.

Acknowledgements

We thank RWE Dea AG, Hamburg for providing a high quality seismic data set and corresponding borehole information. Monika Sobiesiak and Raik Bachmann are thanked for discussions. Constructive reviews from Bruce Trudgill and Michael Edwards are gratefully acknowledged. This study has been funded by the German Science Foundation (DFG SPP 1135 'Sedimentary basin dynamics'; grants Kr2073/1 and Ta427/1).

References

Barnett, J.A.M., Mortimer, J., Rippon, J.H., Walsh, J.J., Watterson, J., 1987. Displacement geometry in the volume containing a single normal fault. AAPG Bulletin 71 (8), 925–937.

Betz, D., Führer, F., Greiner, G., Plein, E., 1987. Evolution of the Lower Saxony Basin. Tectonophysics 137, 127–170.

Bull, J.M., Barnes, P.M., Lamarche, G., Sanderson, D.J., Cowie, P.A., Taylor, S.K., Dix, J.K., 2006. High-resolution record of displacement accumulation on an active normal fault; implications for models of slip accumulation during repeated earthquakes. Journal of Structural Geology 28 (7), 1146–1166.

Cartwright, J.A., Mansfield, C., Trudgill, B.D., 1996. The growth of normal faults by segment linkage. In: Buchanan, P.G., Nieuwland, D.A. (Eds.), Modern Developments in Structural Interpretation, Validation and Modelling. Geological Society of London, Special Publications, vol. 99. Geological Society of London, United Kingdom, pp. 163–177.

Cartwright, J.A., Trudgill, B.D., Mansfield, C.S., 1995. Fault growth by segment linkage: an explanation for scatter in maximum displacement and trace length data from the Canyonlands Grabens of SE Utah. Journal of Structural Geology 17 (9), 1319–1326.

Crider, J.G., Peacock, D.C.P., 2004. Initiation of brittle faults in the upper crust: a review of field observations. Journal of Structural Geology 26 (4), 691–707.

Coelho, S., Passchier, C., Grasemann, B., 2005. Geometric description of flanking structures. Journal of Structural Geology 27 (4), 597–606.

Exner, U., Mancktelow, N.S., Grasemann, B., 2004. Progressive development of s-type flanking folds in simple shear. Journal of Structural Geology 26 (12), 2191–2201.

Grasemann, B., Martel, S., Passchier, C., 2005. Reverse and normal drag along a fault. Journal of Structural Geology 27 (6), 999–1010.

Hancock, P.L., Barka, A.A., 1987. Kinematic indicators on active normal faults in western Turkey. In: Shear Criteria in Rocks 9. Pergamon, Oxford-New York, International, pp. 573–584.

Kockel, F., 2002. Rifting processes in NW Germany and the German North Sea sector. Netherlands Journal of Geosciences/Geologie en Mijnbouw 81, 149–158.

Lisle, R.J., 1994. Detection of zones of abnormal strains in structures using Gaussian curvature analysis. AAPG Bulletin 78 (12), 1811–1819.

Lohr, T., Krawczyk, C.M., Tanner, D.C., Samiee, R., Endres, H., Oncken, O., Trappe, H., Kukla, P.A., 2007. Strain partitioning due to salt: insights from interpretation of a 3D seismic data set in the NW German Basin. Basin Research 19 (4), 579–597.

Manighetti, I., King, G.C.P., Gaudemer, Y., Scholz, C.H., Doubre, C., 2001. Slip accumulation and lateral propagation of active normal faults in Afar. Journal of Geophysical Research, B, Solid Earth and Planets 106 (7), 13667–13696.

Mansfield, C., Cartwright, J., 2001. Fault growth by linkage: observations and implications from analogue models. Journal of Structural Geology 23 (5), 745–763.

Manzocchi, T., Walsh, J.J., Nicol, A., 2006. Displacement accumulation from earthquakes on isolated normal faults. Journal of Structural Geology 28 (9), 1685–1693.

Marchal, D., Guiraud, M., Rives, T., 2003. Geometric and morphologic evolution of normal fault planes and traces from 2D to 4D data. Journal of Structural Geology 25 (1), 135–158.

McLeod, A.E., Dawers, N.H., Underhill, J.R., 2000. The propagation and linkage of normal faults: insights from the Strathspey-Brent-Statfjord fault array, northern North Sea. In: Processes and Controls in the Stratigraphic Development of Extensional Basins. Basin Research, vol. 12. Blackwell Science, Oxford, United Kingdom, pp. 263–284.

Meyer, V., Nicol, A., Childs, C., Walsh, J.J., Watterson, J., 2002. Progressive localisation of strain during the evolution of a normal fault population. Journal of Structural Geology 24 (8), 1215–1231.

Needham, T., Yielding, G., Freeman, R., 1996. Analysis of fault geometry and displacement patterns. In: Buchanan, P.G., Nieuwland, D.A. (Eds.), Modern Developments in Structural Interpretation, Validation and Modelling. Geological Society of London, Special Publications, vol. 99. Geological Society, London, pp. 189–199.

Nicol, A., Walsh, J., Berryman, K., Nodder, S.D., 2005. Growth of a normal fault by the accumulation of slip over millions of years. Journal of Structural Geology 27 (2), 327–342.

Nicol, A., Walsh, J.J., Watterson, J., Gillespie, P.A., 1996. Fault size distributions – are they really power-law?. In: Special Issue; Scaling Laws for Fault and Fracture Populations; Analyses and Applications, vol. 18. Pergamon, Oxford-New York, International, pp. 191–197.

Passchier, C.W., 2001. Flanking structures. In: Evolution of Structures in Deforming Rocks; in Honour of Paul F Williams, vol. 23. Pergamon, Oxford, International, pp. 951–962.

Peacock, D.C.P., Sanderson, D.J., 1991. Displacements, segment linkage and relay ramps in normal fault zones. Journal of Structural Geology 13 (6), 721–733.

Peacock, D.C.P., Knipe, R.J., Sanderson, D.J., 2000. Glossary of normal faults. Journal of Structural Geology 22 (3), 291–305.

Sagy, A., Brodsky, E.E., Axen, G.J., 2007. Evolution of fault-surface roughness with slip. Geology 35 (3), 283–286.

Scholz, C.H., 2002. The Mechanics of Earthquakes and Faulting. Cambridge University Press.

Sobiesiak, M., Meyer, U., Schmidt, S., Götze, H.-J., Krawczyk, C.M., 2007. Asperity generating upper crustal sources revealed by *b* value and isostatic residual anomaly grids in the area of Antofagasta, Chile. Journal of Geophysical Research 112, B12308, doi:10.1029/2006JB004796.

Walsh, J.J., Nicol, A., Childs, C., 2002. An alternative model for the growth of faults. Journal of Structural Geology 24 (11), 1669–1675.

Walsh, J.J., Watterson, J., 1989. Displacement gradients on fault surfaces. Journal of Structural Geology 11 (3), 307–316.

Walsh, J.J., Watterson, J., Bailey, W.R., Childs, C., 1999. Fault relays, bends and branch-lines. Journal of Structural Geology 21 (8–9), 1019–1026.

Wiesmayr, G., Grasemann, B., 2005. Sense and non-sense of shear in flanking structures with layer-parallel shortening: implications for fault-related folds. Journal of Structural Geology 27 (2), 249–264.

Willemse, E.J.M., 1997. Segmented normal faults: correspondence between three-dimensional mechanical models and field data. Journal of Geophysical Research, Solid Earth and Planets 102 (1), 675–692.

Wright, T.D., Turner, J.P., 2006. Characterization of 3D fault curvature. In: Geophysical Research Abstracts, vol. 8. EGU, Vienna.

Ziegler, P.A., 1990. Collision related intra-plate compression deformations in Western and Central Europe. Journal of Geodynamics 11 (4), 357–388.